Retinal Basal Laminar Deposits in Complement fH/fP Mouse Model of Dense Deposit Disease

Delu Song,[1] Imran Mohammed,[2] Rupak Bhuyan,[1] Takashi Miwa,[2] Allison Lesher Williams,[2] Damodar Gullipalli,[2] Sayaka Sato,[2] Ying Song,[1] Joshua L. Dunaief,[1] and Wen-Chao Song[2]

[1]Department of Ophthalmology, Perelman School of Medicine, University of Pennsylvania, Philadelphia, Pennsylvania, United States
[2]Department of Systems Pharmacology and Translational Therapeutics, Perelman School of Medicine, University of Pennsylvania, Philadelphia, Pennsylvania, United States

Correspondence: Joshua L. Dunaief, 305 Stellar Chance Labs, 422 Curie Blvd, Philadelphia, PA 19104, USA; jdunaief@mail.med.upenn.edu. Wen-Chao Song, Room 1254 BRBII/III, 421 Curie Boulevard, Philadelphia, PA 19104, USA; songwe@mail.med.upenn.edu.

DS and IM contributed equally to the work presented here and should therefore be regarded as equivalent authors.

Submitted: February 24, 2018
Accepted: May 25, 2018

Citation: Song D, Mohammed I, Bhuyan R, et al. Retinal basal laminar deposits in complement fH/fP mouse model of dense deposit disease. *Invest Ophthalmol Vis Sci*. 2018;59:3405–3415. https://doi.org/10.1167/iovs.18-24133

Purpose. Dense deposit disease (DDD) is caused by dysregulation of the alternative pathway of the complement cascade and characterized by electron-dense deposits in the kidney glomerular basement membrane (GBM) and drusen in Bruch's membrane (BrM). Complement factor H (fH) and factor properdin (fP) regulate complement activation; fH inhibits alternative pathway (AP) activation, whereas fP promotes it. We report pathologic changes in eyes of an fH and fP double-mutant mouse, which we previously showed have dense deposits in the GBM and early mortality from nephropathy.

Methods. $fH^{m/m}$, $fP^{-/-}$, and $fH^{m/m}/fP^{-/-}$ mice were generated on a C57BL/6–129J background. Fundus imaging at 8 weeks of age was followed by analysis via light and electron microscopy. Retinal function was assessed by electroretinography (ERG). Complement levels and localization were tested by immunohistochemistry and ELISA. Retinas of $fH^{m/m}/fP^{-/-}$ mice treated with intraperitoneal injections of an anti-C5 antibody were compared to those of age- and genotype-matched mice injected with an isotype control antibody.

Results. $fH^{m/m}/fP^{-/-}$ mice suffered early-onset retinal hypopigmented spots detected using in vivo retinal photography, and histologic examination showed basal laminar deposits (BLamD), degeneration of the photoreceptors, and RPE vacuolization. ERG showed diminished retinal function. The anti-C5 antibody was retina-protective.

Conclusions. This unique mouse represents a new model of complement-mediated rapid-onset DDD, and could be useful in exploring the pathologic changes associated with BLamD in age-related macular degeneration.

Keywords: factor H, properdin, retinal degeneration, dense deposit disease

Dense deposit disease (DDD) and C3 glomerulonephritis (C3GN) are rare forms of glomerulonephritis that affect children and young adults.[1,2] Both diseases result from abnormal regulation of the alternative pathway of the complement system and are now classified under the heading of "C3 glomerulopathies." DDD (also known as membranoproliferative glomerulonephritis type II) is characterized by electron-dense deposits in the glomerular basement membrane (GBM) as well as drusen in Bruch's membrane (BrM).[1] There currently are no mechanism-directed therapies to treat affected patients, approximately 50% of whom progress to having end-stage renal disease within 10 years of diagnosis.[1] The composition of drusen in patients with DDD is similar to that in patients with age-related macular degeneration (AMD): both types contain lipids, cholesterol, amyloid P component, vitronectin, and complement components C5 and C5b-9.[3,4] This is consistent with the current understanding that DDD and AMD share a complement-mediated pathogenesis.[5] Unlike in AMD, however, drusen in individuals with DDD form at an early age and often are detected in the second decade of life with a variable distribution within the retina.[6–8] Over time, atrophic changes can occur in the neurosensory retina (NSR) and RPE, thereby causing deterioration of vision. Late-stage complications include choroidal neovascularization and central serous retinopathy.[6]

As a component of the innate immune system, complement has a key role in recognizing and fighting infections.[9] Complement is activated via three pathways: the classical, lectin, and alternative pathways (AP). AP dysregulation has been found in many complement-mediated human diseases, including AMD.[10–12] Among several proteins that regulate AP, complement factor H (fH) is an abundant plasma regulator inhibiting the activity of C3 convertase C3bBb on the cell surface and in the fluid phase.[13–15] fH has 20 short consensus repeat (SCR) domains, and the N-terminal SCRs 1 to 4 are responsible for complement regulation. Polymorphisms in fH are associated with AMD, especially the common Y402H variant in SCR 7,[16] which contains the overlapping binding sites for heparin, C-reactive protein (CRP), and streptococcal M protein.[17] C3GN, DDD, and atypical hemolytic uremic syndrome (aHUS) also are associated with fH mutations.[1,2,15,18]

In opposition to fH, properdin, or complement factor P (fP), positively regulates AP activation by stabilizing C3bBb, significantly increasing its half-life.[19] It has 6 thrombospondin type 1 repeat (TSR) domains, and TSRs 5 and 6 mediate its oligomerization and function. fP circulates in plasma and,

unlike any other complement protein, is produced primarily by leukocytes instead of hepatocytes. Accordingly, fP levels are elevated in inflammatory microenvironments.[20] Properdin-deficient mice have been used as models to study arthritis,[21,22] ischemic-reperfusion injury,[23] abdominal aortic aneurysms,[24,25] asthma,[24,26] septic[27] and nonseptic shock,[28] and C3 glomerulopathy.[29,30]

Previously, we created an fH mutant mouse by inserting two stop codons at the beginning of SCR 19 of the *fH* gene to selectively disrupt function of the C-terminal domain of fH to model aHUS-related mutations in this region.[30] Unexpectedly, our fH mutant mouse had impaired fH activity in the fluid phase and on the cell surface due to expression of only a small amount of the truncated fH protein in the plasma, and a nonlethal form of C3 glomerulopathy developed instead of aHUS.[30] When this fH mutant mouse was rendered deficient in fP either by genetic deletion or by antibody neutralization, paradoxically a more severe and lethal form of C3 glomerulopathy developed showing kidney injury on electron microscopy similar to human DDD.[30] We characterized pathologic changes in the retina of this mouse model, finding rapid-onset hypopigmented spots representing RPE degeneration detected by fundus photography, and histologic evidence of sub-RPE basal laminar deposits (BLamD), as well as RPE and photoreceptor (PR) degeneration. Because this unique mouse model exhibits retinal manifestations similar to those in DDD, it could be useful in testing new therapies for DDD and retinopathies containing BLamD.

Materials and Methods

Animals

Generation of $fH^{m/m}$, $fP^{-/-}$ and $fH^{m/m}/fP^{-/-}$ on a C57BL/6–129J mixed background were described previously.[21,30] All mice were housed in a UPenn nonbarrier facility maintained at 21-23°C, a 12-hour/12-hour light-dark cycle, and free access to food and water. All experiments used age-matched littermates as controls. Mice were negative for the *rd1* and *rd8* mutations. Experimental procedures were performed in accordance with the Association for Research in Vision and Ophthalmology (ARVO) Statement for the Use of Animals in Ophthalmology and Vision Research. All protocols were approved by the animal care review board of the University of Pennsylvania. Most $fH^{m/m}/fP^{-/-}$ mice had to be euthanized between 8 and 12 weeks due to renal failure.[30] However, all mice used in this study were not critically moribund.

Fundus Imaging

Mice were anesthetized with a single intraperitoneal injection of ketamine (80 mg/kg) xylazine (40 mg/kg), and acepromazine (2 mg/kg). Pupils then were dilated with 1% tropicamide (Mydriacyl; Alcon, Fort Worth, TX, US). Once sufficiently anesthetized, mice were placed on a padded metal stage. Color and autofluorescence images then were acquired using a fundus camera (Micron III; Phoenix Research Laboratories, Inc., Pleasanton, CA, USA).

Morphologic Analysis

Electron microscopy on retinal samples was performed as described previously.[31] After enucleation, eyes were fixed in 2% paraformaldehyde/2% glutaraldehyde overnight at 4°C. The anterior segment was removed, and the posterior portion of each eye was cut into small wedge-shaped pieces and post-fixed in 1% osmium tetroxide/0.1 mol/L sodium cacodylate buffer, dehydrated, and embedded in EMbed-812 (Electron Microscopy Sciences, Hatfield, PA, USA). Ultrathin sections (60–80 nm thick) were stained and examined with a JEOL1010 transmission electron microscope (JEOL Ltd., Tokyo, Japan). Images were acquired with Advanced Microscopy Techniques Image Capture software version 602 (Advanced Microscopy Techniques Corp., Woburn, MA, USA) and were rotated and cropped with Adobe Photoshop CS5 (Adobe Systems Incorporated, San Jose, CA, USA).

The following strategy was used to quantify RPE and BrM degeneration.[32] (1) Continuity of sub-RPE deposits: 0, no deposits; 1, occasional deposits; 2, deposits extending <2 RPE cells; 3, deposit extending ≥ 2 RPE cells. (2) Thickness of deposits: 0, no deposits; 1, flat deposits; 2, thickness of deposits $<25\%$ of RPE thickness; 3, thickness of deposits $>25\%$ of RPE thickness. (3) Nature of deposit content: 0, no deposits; 1, homogenous deposit; 2, banded structure in deposits; 3, ≥ 3 banded structures in deposits. (4) BrM abnormality: 0, normal; 1, collagenous thickening without deposits; 2, thickening with circular profiles or nonspecific debris; 3, banded structures, granular material or membranous debris. Severity score of 0 to 12 was determined on each specimen by adding the scores of the aforementioned categories. Scoring was performed for 10 micrographs per eye at $\times$20,000 magnification at equal intervals, and a mean score for each eye was calculated. One eye was analyzed from each mouse.

Light Microscopy on Retinal Plastic Sections

Enucleated eyes were immersion-fixed in 2% paraformaldehyde/2% glutaraldehyde overnight at 4°C. The tissues then were dehydrated in increasing concentrations of ethanol, infiltrated overnight, and embedded the next day in a water-soluble, 2-hydroxyethyl methacrylate (HEMA) plastic resin (JB4 Solution A, Polysciences, Inc., Warrington, PA, USA). For standard histology, 3-μm thick plastic sections were cut in the sagittal plane and toluidine blue–stained as described previously.[31] The number of nuclei per column of outer nuclear layer (ONL) PRs was counted in triplicate at 200 μm intervals from the optic nerve head (ONH) to 1800 μm from the ONH, using image analysis software (ImagePro Plus 4.1; Media Cybernetics, Silver Spring, MD, USA) to calculate distances from manually set lengths.

Immunofluorescence

After the globes were fixed in 4% paraformaldehyde, eyecups were generated by removing the anterior segment. The eyecups were infiltrated in 30% sucrose overnight and embedded in Tissue-Tek O.C.T. compound (Sakura Finetek, Torrance, CA, USA). Immunofluorescence was performed on sections 10 μm thick as described previously.[31] After incubation with FITC-conjugated goat anti-mouse C3 antibody (#0855500 MP Biomedicals, Solon, OH, USA) and anti-rhodopsin antibody (ab5417, Abcam, Cambridge, MA, USA), the sections were analyzed by fluorescence microscopy with identical exposure parameters (model TE300 microscope; Nikon, Tokyo, Japan) with ImagePro software (Media Cybernetics). Control sections were treated with a goat IgG FITC-isotype antibody (ab37374; Abcam).

Electroretinography (ERG)

ERG recordings were performed as described previously.[33] In brief, mice were dark-adapted overnight and then anesthetized with a mixture delivering (in mg/kg body weight) 100 ketamine, 2 xylazine, and 2 acepromazine. After pupils were dilated, and mice were placed on a stage maintained at 37°C. The ERG apparatus was modified by the manufacturer for experiments with mice by

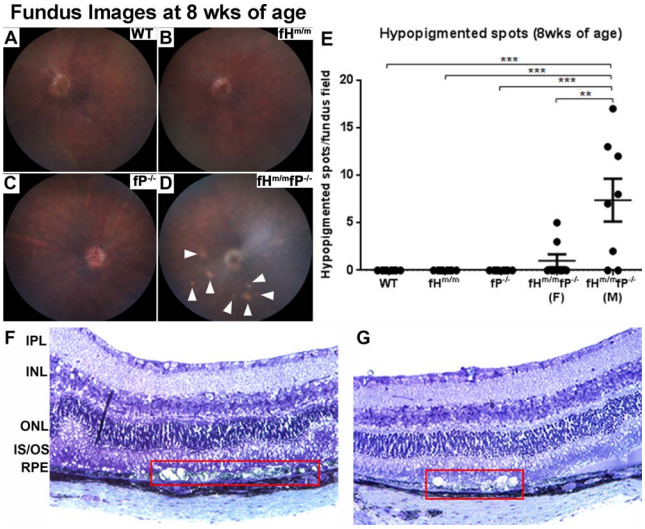

Figure 1. Fundus photographs and plastic sections at 8 weeks of age. Images for (**A**) WT, (**B**) $fH^{m/m}$, (**C**) $fP^{-/-}$, and (**D**) $fH^{m/m}/fP^{-/-}$ mice. *Arrowheads* denote hypopigmented lesions. (**E**) Numbers of hypopigmented lesions per fundus field. Male $fH^{m/m}/fP^{-/-}$ mice ($n = 8$) had significantly more lesions than female $fH^{m/m}/fP^{-/-}$ mice ($n = 8$) and other genotypes ($n = 8$ in WT, $fH^{m/m}$, and $fP^{-/-}$). Plastic sections revealed RPE vacuolization at the locations corresponding to hypopigmented lesions displayed on fundus images (**F**, **G**; *red frames*) $^{**}P < 0.01$; $^{***}P < 0.001$. *Scale Bars*: mean ± SEM. IPL, inner plexiform layer; INL, inner nuclear layer.

substituting light-emitting diodes with emission maximum at 365 nm for standard blue ones. The stage was positioned in such a way that the mouse's head was located inside the stimulator (Color-Dome; Diagnosys LLC, Lowell, MA, USA); thus, ensuring uniform full-field illumination.

C5 ELISA

To measure levels of intact C5, 96-well ELISA plates were coated with 5 µg/mL anti-mouse C5 monoclonal antibody (mAb) BB5.1 in 0.1 M carbonate buffer overnight at 4°C. Plates were washed after each step with PBS/0.5% Tween-20 (PBS-T). Plates then were blocked with 1% BSA-PBS for 1 hour at room temperature (RT) followed by addition of serially diluted mouse plasma samples in 1% BSA-PBS starting at 1:10. After incubation with plasma for 1 hour at RT, the plate was washed three times with PBS-T and then incubated with horseradish peroxidase goat polyclonal anti-human C5 Ab (cross-reacts with mouse C5, 1:1000; Quidel, CA, USA) for 1 hour at RT. After washing, the plate was developed using OptEIA substrate (BD Biosciences, San Jose, CA, USA).

Anti-C5 Antibody Treatment

$fH^{m/m}/fP^{-/-}$ mice were treated systemically by intraperitoneal administration of an anti-C5 mAb (BB5.1), 1 mg twice weekly for 12 weeks starting at 4 weeks of age. All mice weighed 20-25 g during injections. Mice in the control group were treated with an isotype control mAb (purified from MoPC-31C hybridoma; American Type Culture Collection [ATCC], Manassas, VA, USA) at the same dosage and frequency but only for 4 weeks due to early mortality from kidney disease.

Statistical Analysis

The means ± SEM were calculated for each comparison pair. Statistical analyses for hypopigmented spot counting, ERG and C5 ELISA were performed in GraphPad Prism 6.0 (San Diego, CA, USA) using the 1-way ANOVA with a Tukey post hoc test comparing the mean of each group with the mean of every other group. ONL thickness (nuclei) in plastic sections were compared using 1-way ANOVA with post hoc pairwise comparisons using Bonferroni adjustment. $P < 0.05$ was considered statistically significant.

Results

$fH^{m/m}/fP^{-/-}$ Mice had Hypopigmented Lesions Detected by Fundus Photography at 8 Weeks of Age

To profile ophthalmic changes, we performed fundus photography of mice at 8 weeks of age. No apparent pathology was noted on fundus photographs of wild type (WT; $n = 8$, Fig. 1A), $fH^{m/m}$ ($n = 8$, Fig. 1B), and $fP^{-/-}$ ($n = 8$, Fig. 1C) mice. However, hypopigmented spots were observed in $fH^{m/m}/fP^{-/-}$ mice ($n = 16$; Fig. 1D, white arrowheads). Hypopigmented spots were visible as early as age 4 weeks. The numbers of hypopigmented lesions then were quantified and analyzed. Interestingly, male $fH^{m/m}/fP^{-/-}$ mice ($n = 8$) had significantly higher numbers of lesions than female $fH^{m/m}/fP^{-/-}$ ($n = 8$) or other genotype ($n = 8$ for each, Fig. 1E) mice. If the observed hypopigmentation involved activation of complement factor C5, the sex difference in $fH^{m/m}/fP^{-/-}$ mice would agree with previous studies showing male mice to have higher basal serum C5 levels than females.[34,35] No significant differences were observed between sexes in WT, $fH^{m/m}$, and $fP^{-/-}$mice (data not shown). Histologic studies demonstrated that those hypopigmented spots are vacuolar degeneration of the RPE (Figs. 1F, 1G, red frames).

Electron Microscopy (EM) Revealed RPE and BrM Abnormalities in $fH^{m/m}/fP^{-/-}$Mice at 8 Weeks of Age

EM was performed to compare WT (Figs. 2A, 2B) and $fH^{m/m}/fP^{-/-}$ (Figs. 2C–J) mice. $fH^{m/m}/fP^{-/-}$ mice exhibited hypertrophic RPE cells (Fig. 2C, arrowhead) with subretinal debris (Fig. 2C, arrows). Some RPE cells in $fH^{m/m}/fP^{-/-}$ mice contained vacuoles (Figs. 2D, 2I, 2J, asterisks) and also more melanosomes (Fig. 2D) than RPE cells in WT (Fig. 2B). Other $fH^{m/m}/fP^{-/-}$ RPE cells contained fewer melanosomes (Fig. 2E) as well as melanosome aggregates (Figs. 2E, 2F, arrows). Additional observations included extruded PR nuclei in the outer segment layer (Fig. 2G, arrow) and deposits (Figs. 2D, 2F, 2H, circles) located between the RPE plasma membrane (Figs. 2B, 2D, 2F, 2H, green arrowheads) and elastic layer of BrM (Figs. 2B, 2D, 2F, 2H, black arrowheads). Given the location of the deposits, these appear to be BLamD, which were patchy and present in approximately one-third of imaged sections. They were more prevalent near the optic nerve and in the mid-periphery, and rare in the periphery. They were not correlated with hypopigmented spots on fundus photography nor with RPE and PR abnormalities.

High magnification images of RPE and BrM revealed normal morphology in WT (Fig. 3A), $fH^{m/m}$ (Fig. 3B), and $fP^{-/-}$ (Fig. 3C) mice. In comparison, $fH^{m/m}/fP^{-/-}$ mice exhibited BLamD (Figs. 3D, 3F, arrows) and BrM thickening (Fig. 3E). To quantify this RPE and BrM degeneration, we categorized and scored each EM image, revealing that $fH^{m/m}$ mice ($n = 3$) and $fP^{-/-}$ mice ($n = 3$) had severity scores that were significantly higher than those of WT ($n = 4$, Fig. 3G; $^{*}P < 0.05$) mice. Female ($n = 4$) $fH^{m/m}/fP^{-/-}$ mice had significantly higher severity scores than WT and a higher mean score than those of $fH^{m/m}$ and $fP^{-/-}$ mice ($^{*}P < 0.05$, $^{***}P < 0.001$). Notably, the severity score of

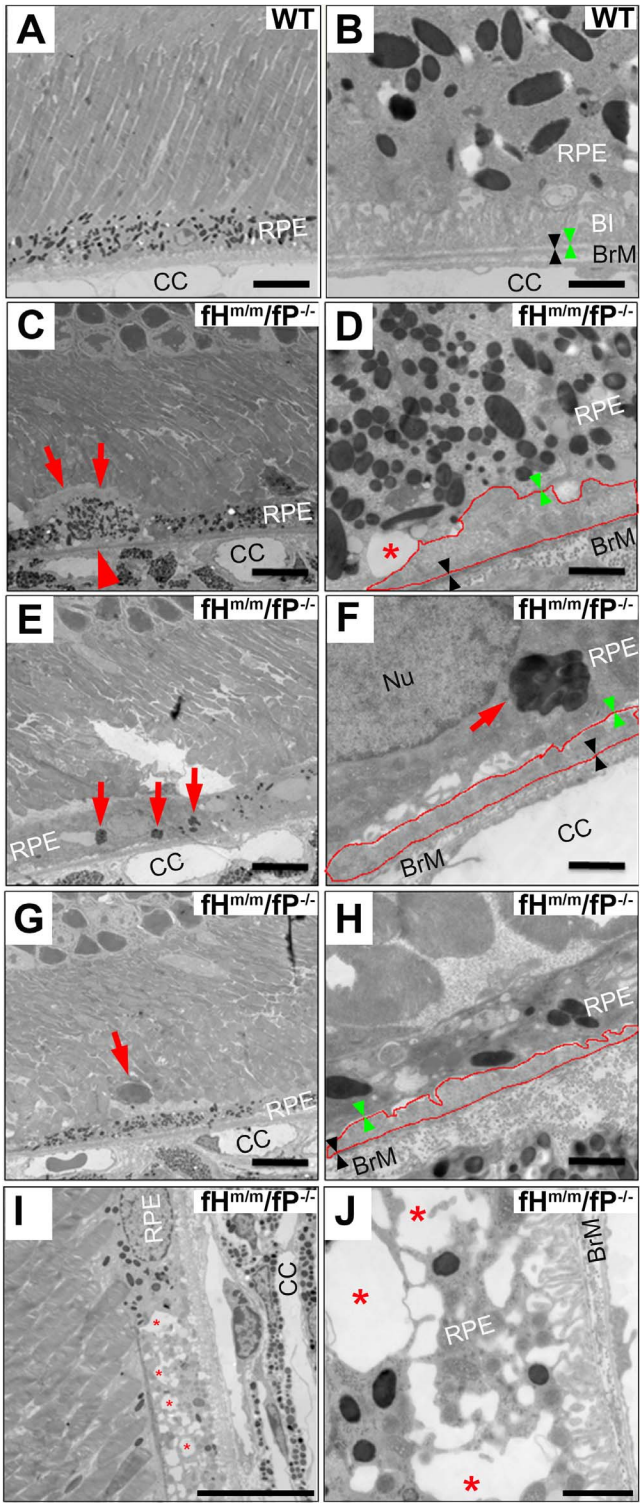

Figure 2. EM analysis on WT and $fH^{m/m}/fP^{-/-}$ retinas. Low (*left column*) and high (*right column*) magnification EMs compare (**A**, **B**) WT to (**C**–**J**) $fH^{m/m}/fP^{-/-}$ mice. (**C**) $fH^{m/m}/fP^{-/-}$ mice exhibited hypertrophic RPE cells (*arrowhead*) with subretinal debris (*arrows*). (**D**) Some RPE cells in $fH^{m/m}/fP^{-/-}$ mice contained more melanosomes compared to WT, and also contained vacuoles (*asterisk*). (**E**) Other RPE cells had fewer melanosomes compared to WT. (**F**) Some RPE cells contained melanosome aggregates (*arrow*). (**G**) Extruded PR nuclei migrating toward the RPE were noted (*arrow*). (**I**, **J**) Multiple vacuoles (*asterisks*) were found in the RPE cells. (**D**, **F**, **H**) Basal laminar deposits (*circles*) were observed. (**B**, **D**, **F**, **H**) *Green arrowheads* indicate the basolateral RPE plasma membrane. *Black arrowheads* indicate the elastic layer of BrM. (**A**, **C**, **E**, **G**, **I**) *Scale bar*: 10 µm. (**B**, **D**, **F**, **H**, **J**) *Scale bar*: 1.5 µm. CC, choriocapillaris; BI, basal infolding; Nu, nucleus.

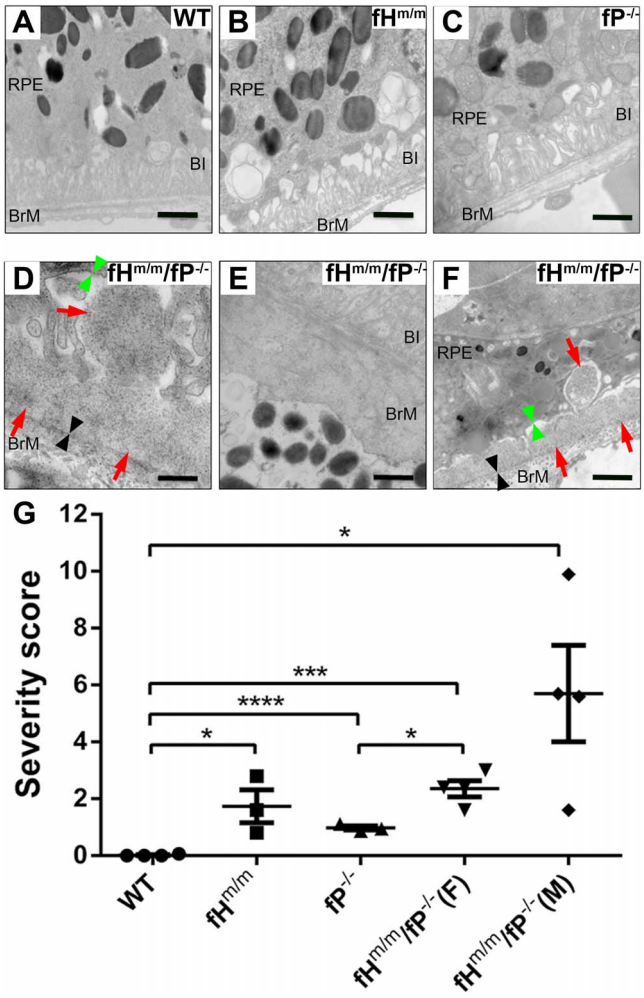

Figure 3. High magnification (×20,000) EM images of RPE and BrM. Normal morphology in (**A**) WT (**B**) $fH^{m/m}$ mice, and (**C**) $fP^{-/-}$ mice. In contrast, (**D**–**F**) $fH^{m/m}/fP^{-/-}$ mice exhibited basal laminar deposits (*arrows*) located between the basolateral RPE plasma membrane (*green arrowheads*) and elastic layer of BrM (*black arrowheads*), as well as (**E**) BrM thickening. *Scale bar*: 1.5 µm. (**G**) Pathologic severity score calculations (maximum score = 12). WT mice ($n = 4$) exhibited little, if any, pathology (severity score 0.02 ± 0.02). $fH^{m/m}$ mice ($n = 3$) exhibited mild pathology (1.73 ± 0.58), as did $fP^{-/-}$ mice ($n = 3$; 0.97 ± 0.07). $fH^{m/m}/fP^{-/-}$ female mice ($n = 4$) had somewhat worse degeneration than $fH^{m/m}$ and $fP^{-/-}$ mice (2.35 ± 0.29). However, $fH^{m/m}/fP^{-/-}$ male mice ($n = 4$) had considerably greater degeneration and much wider variability in scores than all three previous groups (5.70 ± 1.70). $^{*}P < 0.05$, $^{***}P < 0.001$. Severity scores are presented as mean ± SEM.

male $fH^{m/m}/fP^{-/-}$ mice (5.70 ± 1.70) was much higher than that of females (2.35 ± 0.29), although there was larger variation in severity scores within the male group.

Histology Showed PR Death and RPE Degeneration in $fH^{m/m}/fP^{-/-}$ Mice at 8 Weeks of Age

Morphologic analysis was performed at 8 weeks of age. Plastic sections of WT (Fig. 4A), $fH^{m/m}$ (Fig. 4B), and $fP^{-/-}$ (Fig. 4C) mice revealed normal retinal morphology. In contrast, sections from $fH^{m/m}/fP^{-/-}$ mice revealed ONL thinning (Fig. 4D), and disrupted inner and outer segments (Fig. 4E) in $fH^{m/m}/fP^{-/-}$ mice. Finally, ONL thickness measurement via counting of PR

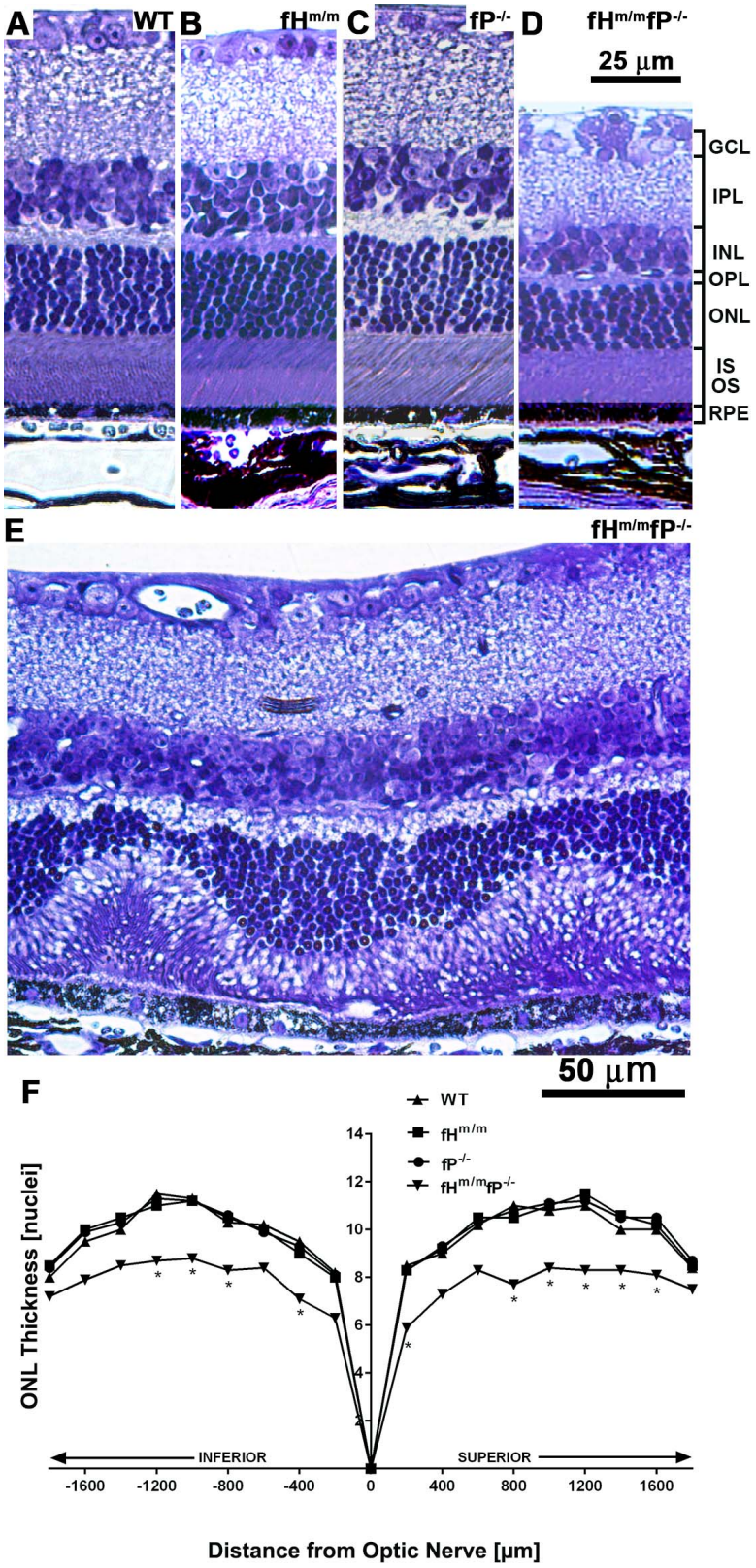

Figure 4. Morphometric analysis of plastic sections from male mouse retinas. Photomicrographs of plastic sections from (**A**) WT, (**B**) fH$^{m/m}$, and (**C**) fP$^{-/-}$ mice revealed normal retinal histology. In contrast, sections from (**D–F**) fH$^{m/m}$/fP$^{-/-}$ mice demonstrated (**D**) ONL thinning, and (**E**) disrupted IS and OS. (**F**) ONL thickness was measured via counting of PR nuclei per column. Measurements were made in triplicate at intervals of 200 μm for a total range of 2000 μm on either side of the optic nerve (reference point 0 on the *x*-axis). There were no significant differences among WT ($n = 3$), fH$^{m/m}$ ($n = 3$), and fP$^{-/-}$ ($n = 3$) mice. In comparison, the ONL in fH$^{m/m}$/fP$^{-/-}$ mice ($n = 3$) was significantly thinner. *Asterisks* represent significant differences between fH$^{m/m}$/fP$^{-/-}$ and WT mice. $^{*}P < 0.05$. (**A–D**) *Scale bar*: 25 μm. (**E**) *Scale bar*: 50 μm. GCL, ganglion cell layer.

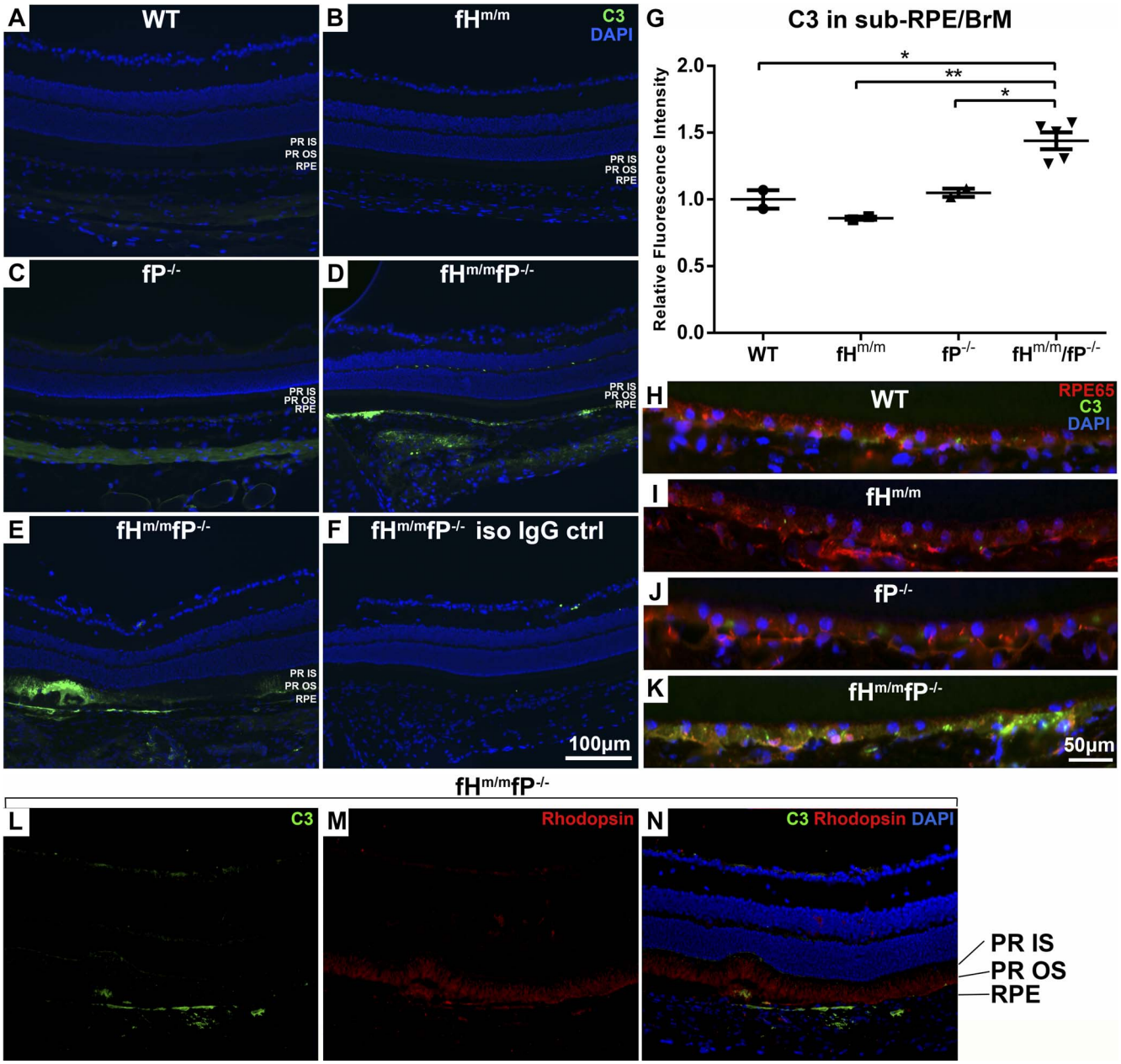

Figure 5. Fluorescence photomicrographs showed more C3 staining in fH$^{m/m}$/fP$^{-/-}$ mice. Relative to (**A**) WT, (**B**) fH$^{m/m}$, (**C**) fP$^{-/-}$, and (**F**) labeling with isotype control antibody in fH$^{m/m}$/fP$^{-/-}$ retinas, the C3 signal in (**D**, **E**) fH$^{m/m}$/fP$^{-/-}$ mice was more striking and localized in (**D**) sub-RPE areas, choroid, and (**E**) PR outer segments. (**G**) Mean pixel density of fluorescence showed that C3 signal in the sub-RPE/BrM region was significantly higher in fH$^{m/m}$/fP$^{-/-}$ ($n = 5$) than in other genotype ($n = 2$ in WT, fH$^{m/m}$, and fP$^{-/-}$) mice. *$P < 0.05$; **$P < 0.01$. *Scale bars*: mean ± SEM. (**H**–**K**) Higher magnification images with RPE65 staining showed that the C3 signal is more prominent under the RPE cells in (**K**) fH$^{m/m}$/fP$^{-/-}$ compared to (**H**) WT, (**I**) fH$^{m/m}$, and (**J**) fP$^{-/-}$ mice. In contrast with rhodopsin signal in PR OS (**M**), C3 is localized in the OS and sub-RPE region (**L**, **N**). (**A**–**F**, **L**–**N**) *Scale bar*: 100 µm. (**H**–**K**) *Scale bar*: 50 µm.

nuclei revealed a significantly thinner ONL in fH$^{m/m}$/fP$^{-/-}$ mice compared to other genotypes (Fig. 4F).

Fluorescence Photomicrographs Showed Increased C3 Staining in fH$^{m/m}$/fP$^{-/-}$ Mice

Previously, deposition of C3 in the kidneys of fH$^{m/m}$ mice was found in mesangium and along the capillary loops of glomeruli. However, C3 staining was brighter and restricted to the capillary loops in glomeruli of fH$^{m/m}$/fP$^{-/-}$ mice.[30] To determine whether the retina also had C3 deposits, we performed immunolabeling for C3 in the retina (Fig. 5). Compared to WT, fH$^{m/m}$, and fP$^{-/-}$ mice (Figs. 5A–C), we detected prominent sub-RPE C3 deposition in fH$^{m/m}$/fP$^{-/-}$ mice (Figs. 5D, 5E, 5K, 5L). Choroidal labeling also was observed in some fH$^{m/m}$/fP$^{-/-}$ mice (Fig. 5D), while in other mice patches of PR outer segments also were stained (Fig. 5E). Higher magnification images that were costained with an antibody against RPE65 further highlighted the sub-RPE C3 deposition in fH$^{m/m}$/fP$^{-/-}$ mice (Figs. 5H–K). Pixel density analysis revealed a significantly increased C3 signal in the sub-RPE/BrM space of fH$^{m/m}$/fP$^{-/-}$ mice (Fig. 5G). Double-labeling with anti-rhodopsin antibody, which labels the PR outer segments (IS/OS; Fig. 5M), confirmed C3 deposits in the sub-

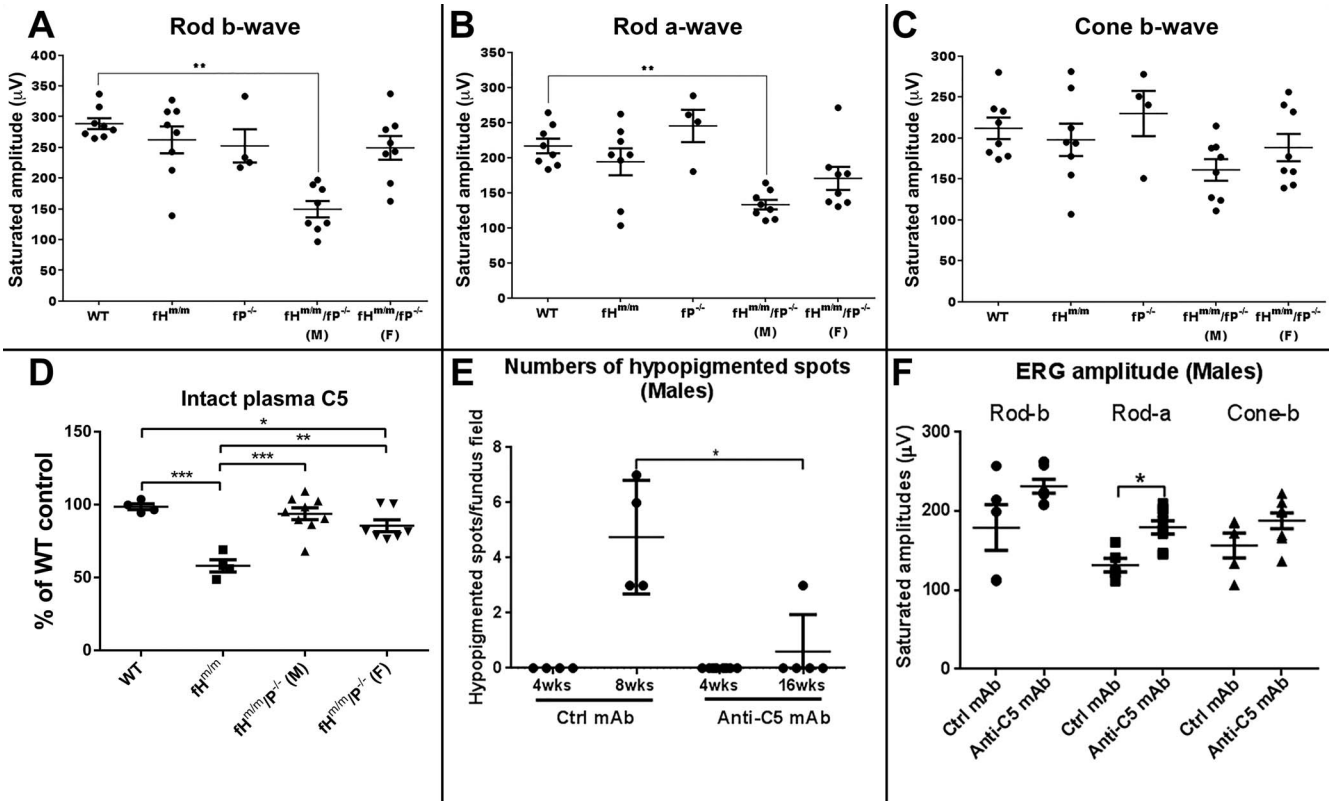

Figure 6. ERG and hypopigmented spots in different groups of mice. (**A**) rod-b, (**B**) rod-a, and (**C**) cone b-wave amplitudes were lower in male $fH^{m/m}/fP^{-/-}$ ($n = 8$) compared to female ($n = 8$), $fH^{m/m}$ ($n = 8$), $fP^{-/-}$ ($n = 4$), and WT ($n = 8$) mice. Differences in amplitude for rod-b and rod-a waves between male $fH^{m/m}/fP^{-/-}$ and WT mice were statistically significant. (**D**) male $fH^{m/m}/fP^{-/-}$ ($n = 9$) and female ($n = 7$) mice had significantly higher serum C5 levels than $fH^{m/m}$ mice ($n = 4$), and there was no significant difference in C5 levels between $fH^{m/m}/fP^{-/-}$ male and WT mice ($n = 4$). (**E**) In $fH^{m/m}/fP^{-/-}$ mice that received systemic anti-C5 antibody treatment ($n = 5$), the numbers of hypopigmented spots on fundus imaging were significantly decreased compared to mice treated with control antibody ($n = 4$). (**F**) ERG amplitudes were higher in $fH^{m/m}/fP^{-/-}$mice treated with anti-C5 antibody ($n = 8$) compared to control antibody ($n = 5$), and the rod-a wave amplitude was significantly protected. $^{*}P < 0.05$; $^{**}P < 0.01$, $^{***}P < 0.001$. *Scale bars*: mean ± SEM.

RPE region and in small patches of outer segments (Figs. 5L–N).

ERG Showed Reduced Amplitudes in $fH^{m/m}/fP^{-/-}$ Mice

We performed ERG to assess retinal PR function. The rod-b (Fig. 6A), rod-a (Fig. 6B), and cone b-wave (Fig. 6C) amplitudes were lower in male $fH^{m/m}/fP^{-/-}$ mice relative to females and to the other genotypes. The reduction relative to WT was significant in rod-b and rod-a waves (Figs. 6A, 6B; $^{**}P < 0.01$).

Properdin Deficiency Increases Plasma C5 Levels in $fH^{m/m}$ Mice and Anti-C5 Antibody can Rescue the Retinal Degeneration

Previously, we found a significant increase of intact C3 and C5 in the plasma of $fH^{m/m}/fP^{-/-}$ mice compared to $fH^{m/m}$ mice, indicating that fP deficiency partially decreased AP and terminal complement consumption.[30,36] Restoration of plasma C5 in $fH^{m/m}/fP^{-/-}$ mice was confirmed in the current study (Fig. 6D). Male ($n = 9$) and female ($n = 7$) $fH^{m/m}/fP^{-/-}$ mice had significantly higher serum C5 levels than $fH^{m/m}$ mice ($n = 4$, $^{**}P < 0.01$, $^{***}P < 0.001$). There was no significant difference in C5 levels between $fH^{m/m}/fP^{-/-}$ males and WT mice ($n = 4$), whereas levels in $fH^{m/m}/fP^{-/-}$ females were significantly reduced compared to WT mice ($^{*}P < 0.01$). In a previous study of lethal glomerulonephritis in $fH^{m/m}/fP^{-/-}$ mice, we demonstrated that blocking C5 with a monoclonal antibody starting at 4 weeks of age prevented renal disease and death.[36] To determine if rapid onset retinopathy in $fH^{m/m}/fP^{-/-}$ mice also is mediated by C5, we treated a group of $fH^{m/m}/fP^{-/-}$ mice with either an anti-C5 mAb ($n = 8$) or an isotype control mAb ($n = 4$). Specifically, the anti-C5 mAb binds to and inhibits cleavage of intact C5 into C5a and C5b. Each mouse (weighing 20–25 g) received 1 mg of mAb per injection, given that previous studies with the BB5.1 clone showed that 1 mg reduced up to 80% of serum hemolytic activity.[37] Treatment started at 4 weeks of age, continuing for 12 weeks in the anti-C5 mAb group but only 4 weeks in the control mAb group due to early mortality. We found that $fH^{m/m}/fP^{-/-}$ mice treated with the anti-C5 mAb had fewer hypopigmented lesions on fundus photography compared to control antibody-treated mice (Fig. 6E), This significant difference was even more impressive given that the anti-C5 mAb group was 8 weeks older than the control mAb group, potentially allowing for more age-dependent retinal degeneration. Correspondingly, ERG amplitudes also were higher in $fH^{m/m}/fP^{-/-}$ mice treated with anti-C5 mAb (Fig. 6F). In particular, the difference in rod-a wave amplitudes was significant.

Discussion

We reported a mouse model of retinopathy seen in human DDD. Key changes in the eyes of our $fH^{m/m}/fP^{-/-}$ mice that

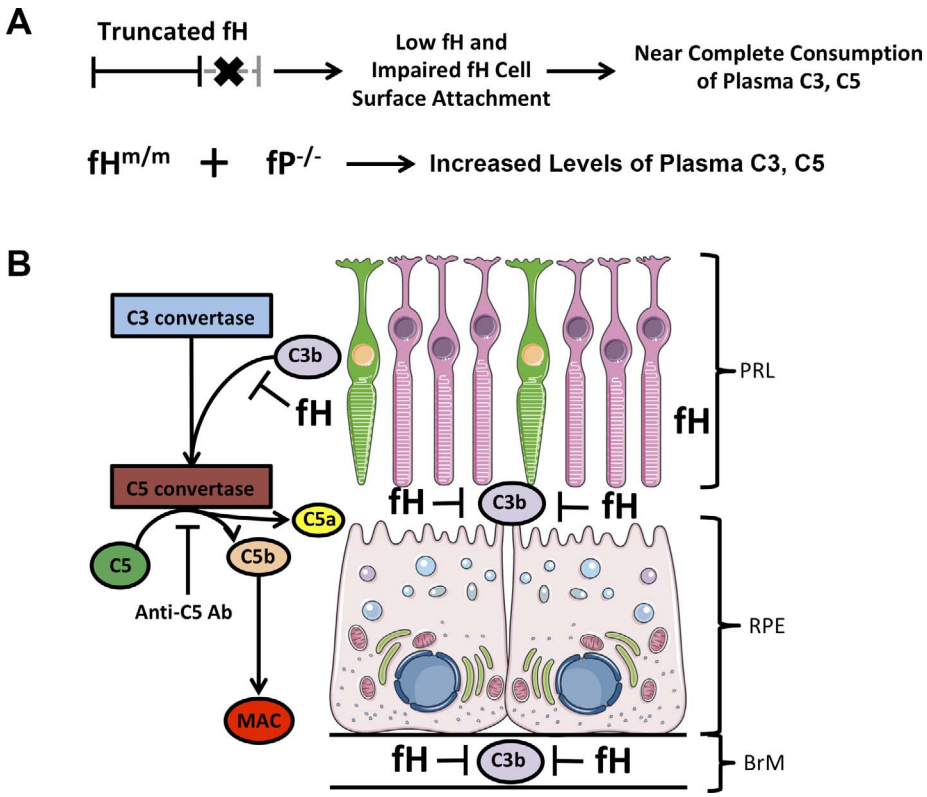

FIGURE 7. Schematic for alternative complement pathway activity in $fH^{m/m}/fP^{-/-}$ mice. (**A**) The fH truncation mutation impaired cell surface attachment and also caused low level expression of fH, resulting in uncontrolled AP complement activation in the fluid phase with near complete C3 and C5 depletion. The fH mutation combined with the fP- knockout reduced fluid phase C3 and C5 consumption and elevated plasma C3 and C5 levels. (**B**) With a low level of truncated fH and impaired fH function, excess AP complement activation occurred in an fP-independent manner, leading to C3b accumulation in the PR IS/OS and sub-RPE/BrM region and terminal complement-mediated local tissue injury. The anti-C5 antibody used in our experiments likely impaired MAC formation, resulting in decreased hypopigmented spots on fundus imaging and improved ERG amplitudes. PRL, PR layer.

mirror human pathology include white spots on fundus imaging, PR death, and RPE pigmentary changes. In addition, we detected reductions in rod-b and –a wave amplitudes on ERG, which also is observed in patients with DDD when they suffer nyctalopia.[38,39]

The choriocapillary–BrM–RPE interface and the capillary tuft–GBM–epithelial interface are strikingly similar, which may explain why DDD patients sometimes have concurrent dense deposit pathology in the kidney and eye.[4] Patients typically do not experience visual symptoms until 10 to 15 years after diagnosis, when retinal atrophy and RPE clumping cause impairments in visual acuity and visual fields. Eventually, a large proportion of patients with DDD have multiple sub-RPE drusen that appear yellowish-white on funduscopy.[8,40,41] The drusen usually are found clustered in the macula, although larger soft drusen in other regions also can be present. These drusen are histopathologically similar to the GBM deposits.[3,4,8] Further loss of visual acuity or fields may result from additional complications, including subretinal neovascularization, retinal detachment, and central serous retinopathy.[42,43]

Ultrastructural analysis in our $fH^{m/m}/fP^{-/-}$ mice revealed BLamD. These deposits form between the RPE and RPE basal lamina as discrete pockets in aging normal eyes, but as a continuous layer in AMD eyes.[44–47] A continuous layer of BLamD under the fovea is considered by some investigators to be a histologic definition of AMD,[48] and has been associated with advanced AMD risk.[45] The primary components of BLamD are fibrous long-spacing collagen, as well as esterified and unesterified cholesterols.[44] It has been hypothesized that by separating the RPE from its basal lamina, BLamD may promote transport of membranous debris into the inner collagenous zone of BrM. This debris then may accumulate and facilitate formation of basal linear deposits and soft drusen.[49]

In addition, BLamD can contain complement components, including C3.[46] Because we detected increased C3 immunolabeling in the BrM of $fH^{m/m}/fP^{-/-}$ mice, complement activation and deposition is likely to contribute to BLamD formation in our model. Moreover, since C3 circulates in serum and is produced/secreted locally by the RPE,[50–52] C3 from both sources may contribute to the observed deposits.

However, BLamD is not limited to AMD eyes. Although the presence of BLamD is 80% sensitive for AMD in eyes over 60 years old, it only has a specificity of 18%.[53] Indeed, BLamD has been identified in various mouse models of aging as a more general marker of RPE stress.[54] Environmental stressors also have caused formation of BLamD, including cigarette smoke exposure[55] and laser photochemical injury[56] in mice on a high-fat diet. In humans, BLamD has been reported in other adult-onset forms of retinal degeneration, including Sorsby fundus dystrophy, late-onset retinal degeneration, and Malattia Leventinese/Doyne's honeycomb retinal dystrophy.[57–59] BLamD was reported previously in an fH knockout mouse model that exhibited pathologic changes in the kidney.[60,61] We added to this observation by showing that the fH/fP double mutant mouse model of lethal DDD had significant BLamD. Further, while the fH knockout mice were characterized at 8 to 24

months, our mice were studied at 8 weeks of age, showing accelerated degeneration.

The aforementioned pathologic changes in $fH^{m/m}/fP^{-/-}$ mice resulted from modifications to the AP of complement that led to increased autologous complement-mediated tissue injury. The fH mutation impaired fH cell surface attachment, and in theory would render retinas more susceptible to complement-mediated damage. However, due to low expression of the truncated fH and consequent lack of sufficient AP complement regulation in the fluid phase, C3 and C5 were largely consumed, and this paradoxically protected the kidney and eye from more severe injury in $fH^{m/m}$ mice (Fig. 7A). Previously, we found that C3 and C5 consumption was reduced in $fH^{m/m}/fP^{-/-}$ mice compared to $fH^{m/m}$ mice,[30,36] suggesting that fP-deficiency resulted in more C3 and C5 available to damage the kidney and eye in an fP-independent manner.[62] With impaired fH, excess C3b accumulated in the PR outer segments and sub-RPE/BrM regions (Fig. 7B). Furthermore, the efficacy of anti-C5 antibody in reducing hypopigmented spots on fundus imaging and improving ERG amplitudes suggested that terminal complement was excessively activated and contributed to the eye phenotype of $fH^{m/m}/fP^{-/-}$ mice.

An important question concerning complement-mediated retinopathy is the relative contributions of local versus systemic complement. Toomey et al.[60] reported that RPE degeneration with vision loss was induced by a high fat diet only in 2-year-old $fH^{+/-}$ mice, but not in $fH^{-/-}$ mice because of retention of serum C3 in $fH^{+/-}$ mice versus complete serum C3 consumption in $fH^{-/-}$ animals.[60] This is consistent with our results showing that higher C3 and C5 levels in $fH^{m/m}/fP^{-/-}$ mice relative to $fH^{m/m}$ mice led to more C3 and C5 activation in the kidney and eye, with consequent degeneration of those tissues. Our finding that administration via intraperitoneal injection of anti-C5 mAb ameliorated local retinopathy in $fH^{m/m}/fP^{-/-}$ mice further supports the role of systemic complement in contributing to retinal injury in the setting of fH dysfunction.

Interestingly, male $fH^{m/m}/fP^{-/-}$ mice exhibited more severe retinal pathology than females. A potential reason for this difference is that male mice have higher baseline serum C5 levels, which has been attributed to differences in sex hormones, such as testosterone.[34,35] In support of this hypothesis, we found that intact C5 levels were significantly lower in female $fH^{m/m}/fP^{-/-}$ compared to WT mice, whereas there was no difference between male $fH^{m/m}/fP^{-/-}$ and WT mice. In addition, there was significant variability in phenotype severity among male $fH^{m/m}/fP^{-/-}$ mice, including two mice with no hypopigmented spots on fundus photographs. This indicated incomplete penetrance of the $fH^{m/m}/fP^{-/-}$ mutations, similar to the penetrance of defects induced by fH mutations in other organs, such as the kidney.

Our finding that anti-C5 mAb therapy ameliorated retinopathy in $fH^{m/m}/fP^{-/-}$ mice suggested that C5 activation participated in the eye pathophysiology of this DDD mouse model. This result is consistent with our recent study showing that blocking C5 also prevented lethal glomerulonephritis in $fH^{m/m}/fP^{-/-}$ mice.[36] A recent study testing anti-C5a therapy in a $fH^{+/-}$ mouse model on a high fat diet showed that the treatment was ineffective.[63] Perhaps an anti-C5 therapy that blocks C5a and membrane attack complex (MAC) formation would be more effective, as in our study. Furthermore, our results suggested a potential therapeutic role for anti-C5 therapy to treat retinopathy associated with DDD. Current guidelines recommend an ophthalmic exam on presentation and annual screenings beginning 10 years after diagnosis, with prompt treatment for neovascular membranes.[42] Investigations of new treatment strategies for DDD-associated retinopathy are especially useful given that increasing survival after renal transplantation will likely increase its prevalence.[6]

In summary, we characterized the $fH^{m/m}/fP^{-/-}$ mouse as a novel model of DDD-related retinopathy, with notable BLamD formation. The efficacy of systemic anti-C5 antibody treatment suggested that serum complement contributes to the observed pathology. This unique mouse represents a new tool to study complement-mediated rapid-onset retinal disease and RPE stress, and is a useful model to study BLamD in the absence of age-related confounding variables. Future directions for research include using electroretinography to assess RPE function in this model, dissecting how complement dysfunction may be associated with melanosome abnormalities, and determining which complement components are necessary for BLamD formation and for RPE/PR degeneration.

Acknowledgments

Supported by National Institutes of Health (NIH; Bethesda, MD, USA) Grants RO1EY023709 (WCS), RO1AI085596 (WCS), and RO1EY023709 (JLD); a grant from the BrightFocus Foundation M2011-051 (WCS); Research to Prevent Blindness (JLD); the FM Kirby Foundation (JLD); the Paul and Evanina Bell Mackall Foundation Trust (a gift in memory of Lee F. Mauger; JLD); and grant KL2TR001879 from the National Center for Advancing Translational Sciences of the NIH (DS).

Disclosure: **D. Song**, None; **I. Mohammed**, None; **R. Bhuyan**, None; **T. Miwa**, None; **A.L. Williams**, None; **D. Gullipalli**, None; **S. Sato**, None; **Y. Song**, None; **J.L. Dunaief**, None; **W.-C. Song**, None

References

1. Smith RJH, Harris CL, Pickering MC. Dense deposit disease. *Mol Immunol*. 2011;48:1604–1610.
2. Servais A, Frémeaux-Bacchi V, Lequintrec M, et al. Primary glomerulonephritis with isolated C3 deposits: a new entity which shares common genetic risk factors with haemolytic uraemic syndrome. *J Med Genet*. 2007;44:193–199.
3. Duvall-Young J, MacDonald MK, McKechnie NM. Fundus changes in (type II) mesangiocapillary glomerulonephritis simulating drusen: a histopathological report. *Br J Ophthalmol*. 1989;73:297–302.
4. Mullins RF, Aptsiauri N, Hageman GS. Structure and composition of drusen associated with glomerulonephritis: implications for the role of complement activation in drusen biogenesis. *Eye Lond Engl*. 2001;15:390–395.
5. D'souza YB, Jones CJP, Short CD, Roberts ISD, Bonshek RE. Oligosaccharide composition is similar in drusen and dense deposits in membranoproliferative glomerulonephritis type II. *Kidney Int*. 2009;75:824–827.
6. Colville D, Guymer R, Sinclair RA, Savige J. Visual impairment caused by retinal abnormalities in mesangiocapillary (membranoproliferative) glomerulonephritis type II ("dense deposit disease"). *Am J Kidney Dis*. 2003;42:E2–E5.
7. Holz FG, Pauleikhoff D, Klein R, Bird AC. Pathogenesis of lesions in late age-related macular disease. *Am J Ophthalmol*. 2004;137:504–510.
8. Duvall-Young J, Short CD, Raines MF, Gokal R, Lawler W. Fundus changes in mesangiocapillary glomerulonephritis type II: clinical and fluorescein angiographic findings. *Br J Ophthalmol*. 1989;73:900–906.
9. Dunkelberger JR, Song W-C. Complement and its role in innate and adaptive immune responses. *Cell Res*. 2010;20:34–50.
10. Thurman JM, Holers VM. The central role of the alternative complement pathway in human disease. *J Immunol*. 2006;176:1305–1310.

11. Holers VM. The spectrum of complement alternative pathway-mediated diseases. *Immunol Rev*. 2008;223:300–316.
12. Song W-C. Complement regulatory proteins and autoimmunity. *Autoimmunity*. 2006;39:403–410.
13. Józsi M, Zipfel PF. Factor H family proteins and human diseases. *Trends Immunol*. 2008;29:380–387.
14. Rodríguez de Córdoba S, Esparza-Gordillo J, Goicoechea de Jorge E, Lopez-Trascasa M, Sánchez-Corral P. The human complement factor H: functional roles, genetic variations and disease associations. *Mol Immunol*. 2004;41:355–367.
15. Atkinson JP, Goodship THJ. Complement factor H and the hemolytic uremic syndrome. *J Exp Med*. 2007;204:1245–1248.
16. Edwards AO, Ritter R, Abel KJ, Manning A, Panhuysen C, Farrer LA. Complement factor H polymorphism and age-related macular degeneration. *Science*. 2005;308:421–424.
17. Giannakis E, Jokiranta TS, Male DA, et al. A common site within factor H SCR 7 responsible for binding heparin, C-reactive protein and streptococcal M protein. *Eur J Immunol*. 2003;33:962–969.
18. Levy M, Halbwachs-Mecarelli L, Gubler MC, et al. H deficiency in two brothers with atypical dense intramembranous deposit disease. *Kidney Int*. 1986;30:949–956.
19. Fearon DT, Austen KF. Properdin: binding to C3b and stabilization of the C3b-dependent C3 convertase. *J Exp Med*. 1975;142:856–863.
20. Blatt AZ, Pathan S, Ferreira VP. Properdin: a tightly regulated critical inflammatory modulator. *Immunol Rev*. 2016;274:172–190.
21. Kimura Y, Zhou L, Miwa T, Song W-C. Genetic and therapeutic targeting of properdin in mice prevents complement-mediated tissue injury. *J Clin Invest*. 2010;120:3545–3554.
22. Dimitrova P, Ivanovska N, Schwaeble W, Gyurkovska V, Stover C. The role of properdin in murine zymosan-induced arthritis. *Mol Immunol*. 2010;47:1458–1466.
23. Miwa T, Sato S, Gullipalli D, Nangaku M, Song W-C. Blocking properdin, the alternative pathway, and anaphylatoxin receptors ameliorates renal ischemia-reperfusion injury in decay-accelerating factor and CD59 double-knockout mice. *J Immunol*. 2013;190:3552–3559.
24. Hourcade DE, Akk AM, Mitchell LM, Zhou H, Hauhart R, Pham CTN. Anti-complement activity of the Ixodes scapularis salivary protein Salp20. *Mol Immunol*. 2016;69:62–69.
25. Zhou H-F, Yan H, Stover CM, et al. Antibody directs properdin-dependent activation of the complement alternative pathway in a mouse model of abdominal aortic aneurysm. *Proc Natl Acad Sci U S A*. 2012;109:E415–E422.
26. Wang Y, Miwa T, Ducka-Kokalari B, et al. Properdin contributes to allergic airway inflammation through local C3a generation. *J Immunol*. 2015;195:1171–1181.
27. Stover CM, Luckett JC, Echtenacher B, et al. Properdin plays a protective role in polymicrobial septic peritonitis. *J Immunol*. 2008;180:3313–3318.
28. Ivanovska ND, Dimitrova PA, Luckett JC, El-Rachkidy Lonnen R, Schwaeble WJ, Stover CM. Properdin deficiency in murine models of nonseptic shock. *J Immunol*. 2008;180:6962–6969.
29. Ruseva MM, Vernon KA, Lesher AM, et al. Loss of properdin exacerbates C3 glomerulopathy resulting from factor H deficiency. *J Am Soc Nephrol JASN*. 2013;24:43–52.
30. Lesher AM, Zhou L, Kimura Y, et al. Combination of factor H mutation and properdin deficiency causes severe C3 glomerulonephritis. *J Am Soc Nephrol JASN*. 2013;24:53–65.
31. Song D, Song Y, Hadziahmetovic M, Zhong Y, Dunaief JL. Systemic administration of the iron chelator deferiprone protects against light–induced photoreceptor degeneration in the mouse retina. *Free Radic Biol Med*. 2012;53:64–71.
32. Cousins SW, Marin-Castaño ME, Espinosa-Heidmann DG, Alexandridou A, Striker L, Elliot S. Female gender, estrogen loss, and Sub-RPE deposit formation in aged mice. *Invest Ophthalmol Vis Sci*. 2003;44:1221–1229.
33. Song D, Song J, Wang C, Li Y, Dunaief JL. Berberine protects against light-induced photoreceptor degeneration in the mouse retina. *Exp Eye Res*. 2016;145:1–9.
34. Cinader B, Dubiski S, Wardlaw AC. Distribution, inheritance, and properties of an antigen, MUB1, and its relation to hemolytic complement. *J Exp Med*. 1964;120:897–924.
35. Churchill WH, Weintraub RM, Borsos T, Rapp HJ. Mouse complement: the effect of sex hormones and castration on two of the late-acting components. *J Exp Med*. 1967;125:657–672.
36. Williams AL, Gullipalli D, Ueda Y, et al. C5 inhibition prevents renal failure in a mouse model of lethal C3 glomerulopathy. *Kidney Int*. 2017;91:1386–1397.
37. Liu J, Miwa T, Hilliard B, et al. The complement inhibitory protein DAF (CD55) suppresses T cell immunity in vivo. *J Exp Med*. 2005;201:567–577.
38. Michielsen B, Leys A, Van Damme B, Missotten L. Fundus changes in chronic membranoproliferative glomerulonephritis type II. *Doc Ophthalmol*. 1990;76:219–229.
39. Kim RY, Faktorovich EG, Kuo CY, Olson JL. Retinal function abnormalities in membranoproliferative glomerulonephritis type II. *Am J Ophthalmol*. 1997;123:619–628.
40. Leys A, Vanrenterghem Y, Van Damme B, Snyers B, Pirson Y, Leys M. Fundus changes in membranoproliferative glomerulonephritis type II. A fluorescein angiographic study of 23 patients. *Graefes Arch Clin Exp Ophthalmol*. 1991;229:406–410.
41. Davis TM, Holdright DR, Schulenberg WE, Turner RC, Joplin GF. Retinal pigment epithelial change and partial lipodystrophy. *Postgrad Med J*. 1988;64:871–874.
42. Leys A, Michielsen B, Leys M, Vanrenterghem Y, Missotten L, Van Damme B. Subretinal neovascular membranes associated with chronic membranoproliferative glomerulonephritis type II. *Graefes Arch Clin Exp Ophthalmol*. 1990;228:499–504.
43. Ulbig MR, Riordan-Eva P, Holz FG, Rees HC, Hamilton PA. Membranoproliferative glomerulonephritis type II associated with central serous retinopathy. *Am J Ophthalmol*. 1993;116:410–413.
44. Curcio CA, Presley JB, Malek G, Medeiros NE, Avery DV, Kruth HS. Esterified and unesterified cholesterol in drusen and basal deposits of eyes with age-related maculopathy. *Exp Eye Res*. 2005;81:731–741.
45. Sarks S, Cherepanoff S, Killingsworth M, Sarks J. Relationship of basal laminar deposit and membranous debris to the clinical presentation of early age-related macular degeneration. *Invest Ophthalmol Vis Sci*. 2007;48:968–977.
46. Lommatzsch A, Hermans P, Müller KD, Bornfeld N, Bird AC, Pauleikhoff D. Are low inflammatory reactions involved in exudative age-related macular degeneration? Morphological and immunhistochemical analysis of AMD associated with basal deposits. *Graefes Arch Clin Exp Ophthalmol*. 2008;246:803–810.
47. Miller JW. Age-related macular degeneration revisited – piecing the puzzle: the LXIX Edward Jackson Memorial Lecture. *Am J Ophthalmol*. 2013;155:1–35.e13.
48. Sarks SH. Ageing and degeneration in the macular region: a clinico-pathological study. *Br J Ophthalmol*. 1976;60:324–341.
49. Curcio CA, Johnson M. Structure, function, and pathology of Bruch's membrane. *Elastic*. 2013;14652:210–213.
50. Luo C, Chen M, Xu H. Complement gene expression and regulation in mouse retina and retinal pigment epithelium/choroid. *Mol Vis*. 2011;17:1588–1597.

51. Luo C, Zhao J, Madden A, Chen M, Xu H. Complement expression in retinal pigment epithelial cells is modulated by activated macrophages. *Exp Eye Res*. 2013;112:93–101.
52. Natoli R, Fernando N, Jiao H, et al. Retinal macrophages synthesize C3 and activate complement in AMD and in models of focal retinal degeneration. *Invest Ophthalmol Vis Sci*. 2017;58:2977–2990.
53. Curcio CA, Millican CL. Basal linear deposit and large drusen are specific for early age-related maculopathy. *Arch Ophthalmol*. 1999;117:329–339.
54. Marmorstein LY, McLaughlin PJ, Peachey NS, Sasaki T, Marmorstein AD. Formation and progression of sub-retinal pigment epithelium deposits in Efemp1 mutation knock-in mice: a model for the early pathogenic course of macular degeneration. *Hum Mol Genet*. 2007;16:2423–2432.
55. Espinosa-Heidmann DG, Suner IJ, Catanuto P, Hernandez EP, Marin-Castano ME, Cousins SW. Cigarette smoke-related oxidants and the development of sub-RPE deposits in an experimental animal model of dry AMD. *Invest Ophthalmol Vis Sci*. 2006;47:729–737.
56. Dithmar S, Sharara NA, Curcio CA, et al. Murine high-fat diet and laser photochemical model of basal deposits in Bruch membrane. *Arch Ophthalmol*. 2001;119:1643–1649.
57. Weber BH, Vogt G, Pruett RC, Stöhr H, Felbor U. Mutations in the tissue inhibitor of metalloproteinases-3 (TIMP3) in patients with Sorsby's fundus dystrophy. *Nat Genet*. 1994;8:352–356.
58. Hayward C, Shu X, Cideciyan AV, et al. Mutation in a short-chain collagen gene, CTRP5, results in extracellular deposit formation in late-onset retinal degeneration: a genetic model for age-related macular degeneration. *Hum Mol Genet*. 2003;12:2657–2667.
59. Stanton JB, Marmorstein AD, Zhang Y, Marmorstein LY. Deletion of Efemp1 is protective against the development of sub-RPE deposits in mouse eyes, deletion of Efemp1 is protective against BLamD. *Invest Ophthalmol Vis Sci*. 2017;58:1455–1461.
60. Toomey CB, Kelly U, Saban DR, Bowes Rickman C. Regulation of age-related macular degeneration-like pathology by complement factor H. *Proc Natl Acad Sci U S A*. 2015;112:E3040–E3049.
61. Ding J-D, Kelly U, Landowski M, et al. Expression of human complement factor H prevents age-related macular degeneration-like retina damage and kidney abnormalities in aged Cfh knockout mice. *Am J Pathol*. 2015;185:29–42.
62. Lesher AM, Nilsson B, Song W-C. Properdin in complement activation and tissue injury. *Mol Immunol*. 2013;56:191–198.
63. Toomey CB, Landowski M, Klingeborn M, et al. Effect of Anti-C5a therapy in a murine model of early/intermediate dry age-related macular degeneration. *Invest Ophthalmol Vis Sci*. 2018;59:662–673.

Investigative Ophthalmology & Visual Science